CORE
Metadata, citation and similar papers at core.ac.uk
Provided by HKU Scholars Hub
The HKU Scholars Hub The University of Hong Kong 香港大學學術庫

Title	A reciprocal relationship between reactive oxygen species and mitochondrial dynamics in neurodegeneration
Author(s)	Hung, HLC; CHENG, SY; Cheung, YT; Wuwongse, SM; Zhang, NQ; Ho, YS; Lee, MYS; Chang, RCC
Citation	Redox Biology, 2018, v. 14, p. 7-19
Issued Date	2018
URL	http://hdl.handle.net/10722/248330
Rights	This work is licensed under a Creative Commons Attribution-NonCommercial-NoDerivatives 4.0 International License.

Redox Biology 14 (2018) 7–19

Contents lists available at ScienceDirect

Redox Biology

journal homepage: www.elsevier.com/locate/redox

Research paper

A reciprocal relationship between reactive oxygen species and mitochondrial dynamics in neurodegeneration

Clara Hiu-Ling Hung[a,c], Sally Shuk-Yee Cheng[a], Yuen-Ting Cheung[a], Suthicha Wuwongse[a], Natalie Qishan Zhang[a], Yuen-Shan Ho[d], Simon Ming-Yuen Lee[c], Raymond Chuen-Chung Chang[a,b,*]

[a] Laboratory of Neurodegenerative Diseases, School of Biomedical Sciences, LKS Faculty of Medicine, The University of Hong Kong, Hong Kong, China
[b] State Key Laboratory of Brain and Cognitive Sciences, The University of Hong Kong, Pokfulam, Hong Kong, China
[c] Institute of Chinese Medical Sciences, University of Macau, Macau, China
[d] School of Nursing, Faculty of Health and Social Sciences, The Hong Kong Polytechnic University, Hung Hom, Kowloon, Hong Kong, China

ARTICLE INFO

Keywords:
Alzheimer's disease
β-amyloid
Mitochondria
Fission and fusion
Drp-1
Neurodegeneration

ABSTRACT

Mitochondrial fragmentation due to fission/fusion imbalance has often been linked to mitochondrial dysfunction and apoptosis in neurodegeneration. Conventionally, it is believed that once mitochondrial morphology shifts away from its physiological tubular form, mitochondria become defective and downstream apoptotic signaling pathways are triggered. However, our study shows that beta-amyloid (Aβ) induces morphological changes in mitochondria where they become granular-shaped and are distinct from fragmented mitochondria in terms of both morphology and functions. Accumulation of mitochondrial reactive oxygen species triggers granular mitochondria formation, while mitoTEMPO (a mitochondria-targeted superoxide scavenger) restores tubular mitochondrial morphology within Aβ-treated neurons. Interestingly, modulations of mitochondria fission and fusion by genetic and pharmacological tools attenuated not only the induction of granular mitochondria, but also mitochondrial superoxide levels in Aβ−treated neurons. Our study shows a reciprocal relationship between mitochondrial dynamics and reactive oxygen species and provides a new potential therapeutic target at early stages of neurodegenerative disease pathogenesis.

1. Introduction

Mitochondria are ubiquitous intracellular organelles that regulate important cellular functions including bioenergetic metabolism, Ca^{2+} homeostasis and apoptosis. Mitochondrial dysfunction is a prominent pathological feature in various age-related neurodegenerative diseases including Alzheimer's disease (AD) [1–6].

The balance between fission and fusion is required for proper mitochondrial functions due to its involvement in the maintenance of mitochondrial DNA, segregation of damaged mitochondria by mitophagy, distribution and movement of mitochondria within the cell, as well as regulation of mitochondrial morphology [7–9]. Mitochondrial fusion is regulated by mitofusins (Mfn1 and Mfn2) and optic atrophy 1 (OPA1) [10–14]; while fission is mediated by dynamin-related protein 1 (Drp1; also known as DLP-1), mitochondrial fission 1 protein (Fis-1) and mitochondrial fission factor (Mff) [15–19]. Recent studies have shown that these proteins contribute to the formation of distinct mitochondrial morphologies under different cell conditions [20,21]. Oxidative stress has also been shown to induce transient changes in mitochondrial morphology as well as fragmentation of the mitochondrial network [22–24]. With prolonged and persistent cellular oxidative damage, interconnected tubular mitochondrial networks are reorganized as small punctate spheres due to extensive fission, resulting in “mitochondrial fragmentation” in apoptosis [25–27].

Mitochondrial network remodelling has been proposed to play an important role in neurodegeneration [5,28]. β-amyloid peptide (Aβ) has been shown to promote mitochondrial fragmentation [29–32]. An imbalance of fission and fusion proteins has been detected in AD

Abbreviations: Aβ, β-amyloid; AD, Alzheimer's disease; Drp1, Dynamin-related protein 1; ER, Endoplasmic reticulum; ER-RFP, Endoplasmic reticulum-targeted dsRed; FCCP, Carbonyl cyanide p-trifluoro-methoxy-phenyl-hydrazine; H_2O_2, Hydrogen peroxide; Mito-KillerRed, KillerRed-dMito; Mito-GFP, Mitochondria-targeted green fluorescent protein; Mito-RFP, Mitochondria-targeted dsRed; Mito-PAGFP, Photoactivable mitochondria-targeted green fluorescent protein; Mff, Mitochondrial fission factor; Mfn, Mitofusin; OPA1, Optic atrophy 1; ROS, Reactive oxygen species; SPA-FRAP, Simultaneous photoactivation and fluorescence recovery after photobleaching; TMRE, Tetramethylrhodamine ethyl ester

* Correspondence to: Laboratory of Neurodegenerative Diseases, School of Biomedical Sciences, LKS Faculty of Medicine, The University of Hong Kong, Rm. L4-49, Laboratory Block, Faculty of Medicine Building, 21 Sassoon Road, Pokfulam, Hong Kong, China.
E-mail address: R.C.C.Chang@hku.hk (R.C.-C. Chang).

http://dx.doi.org/10.1016/j.redox.2017.08.010
Received 10 July 2017; Received in revised form 3 August 2017; Accepted 8 August 2017
Available online 12 August 2017
2213-2317/ © 2017 The Authors. Published by Elsevier B.V. This is an open access article under the CC BY-NC-ND license (http://creativecommons.org/licenses/BY-NC-ND/4.0/).

patients' brains as well [30,33]. Furthermore, disruption in the fission and fusion balance and mitochondrial trafficking have been demonstrated in various AD transgenic mouse models [34–38]. However, the precise mechanism underlying mitochondrial fragmentation in AD remains under debate [31,39]. Previous studies often focus on mitochondrial fragmentation as an indicator for cell death and mitochondrial dysfunction. However, the relationship between mitochondrial morphology and function remains obscure.

Here, we report that Aβ induced unique changes in mitochondrial morphology, which we refer to as granular mitochondria. Aβ-induced granular mitochondria maintained functional integrity and were thus morphologically and functionally distinct from spherical fragmented mitochondria during apoptosis. Oxidative stress induced by Aβ was found to impair mitochondrial dynamics, as revealed by simultaneous photoactivation and fluorescence recovery after photobleaching (SPA-FRAP) imaging. Notably, we show that mitoTEMPO, the mitochondria-targeted superoxide scavenger, and both genetic and pharmacological approaches to inhibit the fission protein Drp1 could abolish the formation of granular mitochondria by Aβ. Interestingly, attenuation of granular mitochondria formation by inhibiting fission could also ameliorate Aβ-induced accumulation of reactive oxygen species (ROS). Our study demonstrates that Aβ induces acute disturbance in mitochondrial dynamics through induction of oxidative stress, which is independent of apoptosis. In addition, mitochondria morphology and oxidative stress reciprocally affects one another in an in vitro model of AD.

2. Materials and methods

2.1. Primary hippocampal culture

Primary culture of hippocampal neurons was prepared from embryonic day 18–19 Sprague-Dawley rats (Laboratory Animal Unit, The University of Hong Kong, accredited by Association for Assessment and Accreditation of Laboratory Animal Care International) as previously described. All experimental protocols involving animals were approved by the Committee on the Use of Live Animals in Teaching and Research (CULATR) at LKS Faculty of Medicine, HKU. Briefly, hippocampi were isolated and mechanically dissociated in ice-cold phosphate buffered saline (Life Technologies) supplemented with glucose (18 mM, Sigma-Aldrich). Neurons were plated onto poly-L-lysine (25 μg/ml, Sigma-Aldrich) coated glass-bottomed confocal dishes (SPL Life Science) and MatTek (MatTek) culture dishes at a density of 1.5×10^5 cells per dish, or at 5×10^4 and $4.5–6 \times 10^5$ cells per well for 12-well and 6-well plates (Iwaki), respectively. Hippocampal neurons were cultured with Neurobasal® medium (Life Technologies) supplemented with B-27® supplement (2%, Life Technologies), GlutaMAX™ (2 mM, Life Technologies), Penicillin/Streptomycin (100 U and 100 mg/ml, Life Technologies) and β-mercaptoethanol (10 μM, Sigma-Aldrich) for 7–9 days at 37 °C in a humidified 5% CO_2 atmosphere. 5-Fluoro-2′deoxyuridine (2 μM, Sigma-Aldrich) was added after one day in culture to inhibit glial proliferation.

2.2. Transfection

Primary hippocampal neurons seeded on glass-bottomed confocal dish were transfected on DIV 5–6 for 2–3 h with Lipofectamine 2000 (Life Technologies) according to the manufacturer's protocol. Drug treatments were performed 24–48 h after transfection. GFP-Mito (mito-GFP) was purchased from Invitrogen (Life Technologies). DsRed2-Mito (mito-RFP, Clontech) was a generous gift from Prof. Siu-Kai Kong (The Chinese University of Hong Kong, Hong Kong). eGFP-BAX and eGFP-$Drp1^{K38A}$ were gifts from Dr. Zheng Dong (Medical College of Georgia, USA). pKillerRed-dMito (mito-KillerRed) was purchased from Evrogen (Evrogen). mito-PAGFP was obtained from Dr. Richard Youle (Addgene plasmid 23348, Addgene).

2.3. Transfection and transduction

Primary hippocampal neurons seeded on glass-bottomed confocal dish were transduced with baculovirus-based CellLight® Mitochondria-GFP, BacMam 2.0 (Invitrogen™) on day 5–6 following seeding. Drug treatments were performed 24–48 h after transfection.

2.4. Preparation of oligomeric Aβ

Aβ peptides were purchased from Yale University and ChinaPeptides, and were prepared as previously described [40]. Briefly, lyophilized Aβ peptide was first dissolved in 1, 1, 1, 3, 3, 3-hexafluoro-2-propanol (Sigma-Aldrich). After evaporation of the peptide solution, anhydrous DMSO was added to the preparation to achieve the stock solution. The peptide solution was then sonicated at room temperature for 30 min. After sonication, Aβ peptides were snap-frozen in liquid nitrogen, and stored at −80 °C until the day of experiment. Presence of monomers, dimers, and oligomers was confirmed by Tris-Tricine gel electrophoresis as shown previously [40]. Aβ peptides were diluted to the indicated working concentration on the day of the experiment.

2.5. Drug treatments

All drug treatments were performed on DIV6-7. Neurons were treated with 10 μM oligomeric Aβ for the indicated hours. MitoTEMPO (2.5 μM; Enzo® Life Sciences), mitochondrial division inhibitor (mdivi-1, 5 μM; Sigma-Aldrich), and Mitochondrial Fusion Promoter M1 (MFPM1, 5 μM; Sigma-Aldrich) were pre-incubated for 1 h prior to Aβ treatment. Neurons were incubated with 10 μM carbonyl cyanide p-trifluoro-methoxy-phenyl-hydrazine (FCCP; Sigma-Aldrich) for 2 h to induce mitochondrial fragmentation. Neurons were treated with H_2O_2 (50 μM; BDH Chemicals) and rotenone (25 nM; Sigma-Aldrich) for 1 h to induce oxidative stress.

2.6. Confocal live cell imaging

Primary hippocampal neurons were grown on coverglass-bottom confocal dishes for confocal live cell imaging. Images were acquired with a LSM 510 Meta inverted laser-scanning confocal microscope (Carl Zeiss) using a ×63 1.4 NA Apochromat objective (Carl Zeiss), with an incubation chamber maintained at 37 °C with 5% CO_2 during the experiments. Confocal Z-stack images were acquired at 0.4 μm intervals for 7 stacks. The excitation wavelengths were 488 nm for GFP; and 543 nm for DsRed2, MitoSOX™ Red, and Rhod-2. TMRE was excited at 800 nm by two-photon excitation (Chameleon, Coherent Inc.).

For light-induced ROS production experiments using mito-KillerRed, regions of interest were manually defined using the LSM 510 software (Carl Zeiss). To induce light-sensitive ROS production in mitochondria, a small region of one z-plane was irradiated using 100% power of the 543 nm laser. Frames were then acquired every 15 min using the 488 nm and 543 nm lasers for 30 min.

For mitochondrial dynamics assays, hippocampal neurons seeded on coverglass bottomed confocal dishes were co-transfected with mito-RFP and mito-PAGFP. Regions of interest were manually defined using the LSM 510 software (Carl Zeiss). Simultaneous photobleaching of mito-RFP and photoactivation of mito-PAGFP (SPA-FRAP) was performed using 10% power of the 800 nm laser by two-photon excitation (Chameleon, Coherent Inc.). After irradiation, images were acquired every 1 min using the 488 nm and 563 nm laser lines for 30 min. The diffusion rate of mito-PAGFP fluorescence was determined by standard deviation of whole-cell fluorescence at each time point using the Multi-measure plugin of Image J (National Institutes of Health, NIH) as previously described [20]. The fluorescence recovery of mito-RFP in the irradiated region was measured using Image J (NIH) and normalized with a non-bleached area.

To study mitochondrial transport in neuronal processes, neurons

were transfected with mito-RFP. Images were acquired with an ×63 1.4 NA oil Apochromat objective (Carl Zeiss) using a Carl Zeiss Axio Observer inverted microscope equipped with a Perkin Elmer UltraView® spinning disk confocal imaging system. Images were taken every 5 s using the 568 nm laser line of an Argon/Krypton laser (Perkin Elmer) for 150 cycles (~12 min) using the Metamorph software (Molecular Devices). Movement of mitochondria were measured using the Imaris software (Imaris 7.5.1, Bitplane) according to the manufacturer's instructions.

Post-acquisition image processing was performed using Adobe Photoshop (Adobe) and Image J (NIH). Pixel intensities of Rhod-2, MitoSOX™ Red and TMRE were measured using Image J (NIH) after background subtraction.

2.7. Quantitative mitochondrial morphometric analysis

For automated morphometric analysis, aspect ratio and circularity of individual mitochondria were measured using a modified version of the mitochondrial morphology plugin of Image J (NIH) developed by Dagda and colleagues [41]. Volume of mitochondria was measured using the Particle Analyser plugin for Image J (NIH). All measurements were calculated from z-axis confocal stacks. To measure individual mitochondrial length, five 5 cm × 5 cm grids were randomly selected from each image and lengths of five randomly chosen mitochondria were measured in each grid (Photoshop, Adobe). Individual mitochondria were then sub-divided into three categories according to their lengths: short (< 0.87 μm), medium-sized (0.87–1.60 μm), and elongated (> 1.6 μm).

2.8. Quantitative mitochondrial functional analysis

Mitochondrial superoxide production was determined by the mitochondria-specific superoxide sensor MitoSOX™ Red (Life Technologies) according to the manufacturer's instructions. Briefly, hippocampal neurons were incubated with MitoSOX™ Red dye (2.5 μM) in dark at room temperature for 5 min, followed by washing with pre-warmed Hanks buffered saline solution (HBSS, pH 7.4; Life Technologies) supplemented with glucose (5.6 mM, Sigma-Aldrich). Mitochondrial Ca^{2+} concentrations were measured using the mitochondrial-specific fluorescent Ca^{2+} dye Rhod-2 A.M. (Rhod-2) (Life Technologies). To facilitate mitochondrial localization, hippocampal neurons were loaded with Rhod-2 (0.5 μM) in HEPES (20 mM)–buffered Neurobasal® medium in dark for 30 min on ice. The dye was then washed by pre-warmed glucose-supplemented HBSS. Mitochondrial membrane potential was monitored by the fluorescence intensity of Tetramethylrhodamine, ethyl ester (TMRE, Life Technologies). Briefly, TMRE (20 nM) was loaded to the cells and incubated in dark for 5 min at room temperature, followed by washing with pre-warmed glucose-supplemented HBSS. ADP/ATP ratio was measured using the ADP/ATP ratio assay kit (BioVision) according to the manufacturer's protocol.

2.9. SDS-PAGE and Western blotting

Primary hippocampal neurons were lysed in lysis buffer (10 mM Tris at pH 7.4, 100 mM NaCl, 1 mM EDTA, 1 mM EGTA, 1 mM NaF, 20 mM $Na_4P_2O_7$, 1% Triton X-100, 1% glycerol, 0.1% SDS, 0.5% deoxycholate, 1 mM phenylmethylsulfonyl fluoride) supplemented with protease inhibitor cocktail (Sigma-Aldrich) and phosphatase inhibitor cocktail (Sigma-Aldrich) as previously described [40]. The extracted proteins were diluted into indicated amounts and separated on 8–12.5% SDS/PAGE and transferred onto polyvinylidene difluoride (PVDF) blotting membranes (BioRad). The membranes were blocked in 5% non-fat milk (Cell Signaling) dissolved in Tris-buffered saline (pH 7.4) containing 0.1% Tween 20 for 1 h at room temperature and probed with different antibodies: anti-DLP1 (1:3000, BD Biosciences), anti-phospho-Drp1 (Ser 616) (1:1000, Cell Signaling), anti-OPA1 (1:1000, BD Biosciences), anti-Mfn1 (1:1000, Novus Biologicals), anti-Mfn2 (1:1000, Sigma-Aldrich), anti-VDAC (1:1000, Cell Signaling), anti-cleaved-caspase-3 (Asp175) (1:1000, Cell Signaling), and anti-β-actin (1:10,000, Sigma-Aldrich). ECL (GE Healthcare) and Western Bright ECL (Advansta) were used to develop the film. Quantification analysis was performed on scanned films using Image J (NIH).

2.10. Mitochondrial fractionation

Mitochondrial fractionation was performed as previously described [42]. Briefly, neurons were lysed in mitochondrial fractionation lysis buffer (20 mM HEPES at pH 7.5, 250 mM sucrosem, 20 mM KCl, 1.5 mM $MgCl_2$, 1 mM EDTA, 1 mM dithiothreitol and 1 mM phenylmethylsulfonyl fluoride) on ice. The cell lysates were then centrifuged at 600 × *g* for 10 min at 4 °C to remove cell debris. Following centrifugation, the supernatant was transferred into a new tube and was centrifuged again at 7000 × *g* for 10 min at 4 °C. The resulting supernatant and pellet after centrifugation were collected as the cytosolic fraction and mitochondrial fraction, respectively

2.11. Statistical analysis

All results are represented as mean ± S.E.M. for the indicated number (n) of independent experiments. All experiments were repeated for at least 3 times. One-way ANOVA test and Kruskal-Wallis test were used for statistical analysis when appropriate using the GraphPad Prism software (GraphPad). Tukey's (for one-way ANOVA) and Dunn's (for Kruskal-Wallis) multiple comparison tests were used as *post hoc* comparisons of individual groups. p values are as indicated in the figure legends.

3. Results

3.1. Aβ induces changes in mitochondrial morphology in cultured hippocampal neurons, which are morphologically distinct from mitochondrial fragmentation

Primary hippocampal neurons were transfected with mitochondria-targeted green fluorescent protein (mito-GFP) to visualize individual mitochondrion using confocal live cell imaging. In control neurons, mitochondria were mostly thread-like in shape, consistent with previous studies [43] (Fig. 1a). As early as 1–2 h following exposure to Aβ, a change in mitochondria morphology was observed as supported by a significant reduction in mitochondrial length when compared with controls (Fig. 1c). To further validate the changes in mitochondrial length, neurons were sub-divided into three groups (short, medium, elongated) according to the mean mitochondrial length [44]. There were significantly higher percentages of transfected neurons with “short" mitochondria following Aβ treatment (Fig. 1d). To investigate if the reduction in length was a result of change in shape or in size, the volume of mitochondria was measured with both total and individual volume of mitochondria, which were found to be stable when compared with control (Fig. 1e). Morphometric analysis revealed an approximate 20% reduction in mitochondrial aspect ratio (major axis: minor axis ratio; a measure of elongation) following exposure to Aβ, suggesting that Aβ-induced granular mitochondria exhibited a rather ”compressed” and elliptical shape when compared to controls (Fig. 1f). Furthermore, Aβ-treated mitochondria had a significantly higher score in circularity when compared with controls (Fig. 1g). It is important to note that there was no significant change in the number of mitochondria per neuron when compared with control (Fig. 1h). Western blot analysis also revealed no significant change in the expression level of the mitochondrial marker voltage-dependent anion channel (VDAC) following exposure to Aβ (Fig. S2). These results suggest that there was no mitochondrial loss despite the morphological changes.

To determine whether Aβ-induced granular mitochondria were

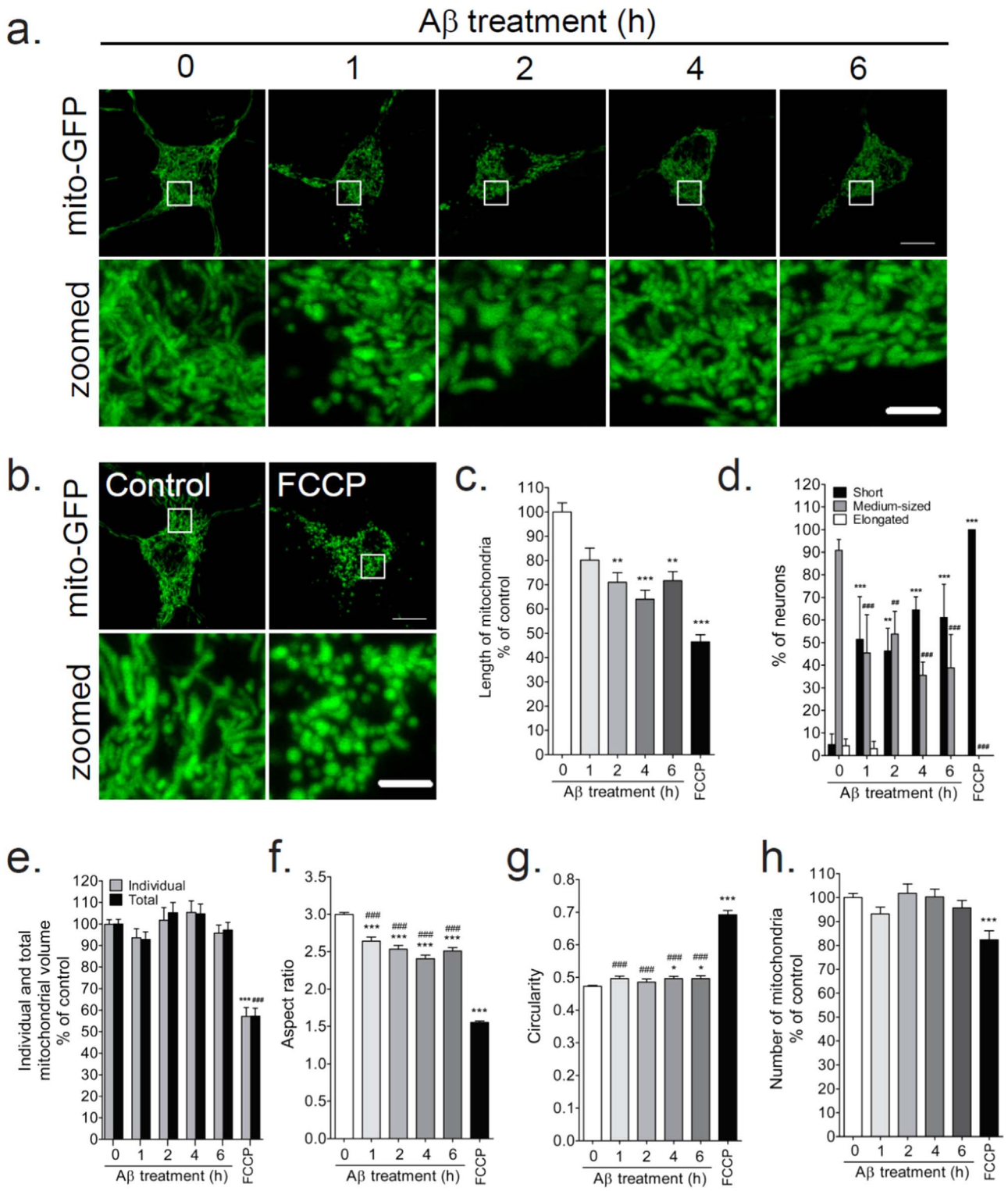

Fig. 1. Aβ induces morphological changes in mitochondria at early time points (1–6 h) which are morphologically different from mitochondrial fragmentation. (a-b) Representative confocal images of mitochondrial morphology 48 h after transfection with mitochondria-targeted GFP (mito-GFP) in rat primary hippocampal neurons to visualize individual mitochondria. Hippocampal neurons were treated with (a) 10 μM Aβ for the indicated periods (in h) or (b) 10 μM FCCP for 2 h to induce mitochondrial fragmentation (Scale bar: 10 μm). Images in the bottom row represent magnification of the boxed areas in the upper row (Scale bar: 2 μm). (c) Percentage of neurons with short (< 0.87 μm), medium-sized (0.87–1.60 μm) and elongated (> 1.60 μm) mitochondria was quantified based on the mean mitochondrial length per neuron. $^{**}/^{\#\#}p < 0.01$, $^{***}/^{\#\#\#}p < 0.001$ compared to control, two-way ANOVA test. (d-h) Statistical quantifications of mitochondrial morphology for each condition, calculated from z-axis confocal stacks. $^{*}p < 0.05$, $^{***}p < 0.001$ compared with control, Kruskal-Wallis test. $^{\#\#}p < 0.01$, $^{\#\#\#}p < 0.001$ compared with FCCP, Dunn's multiple comparison *post-hoc* test. Data represent mean ± SEM of at least 11 independent experiments.

distinct from spherical mitochondria found in apoptosis, potent mitochondrial uncoupler carbonyl cyanide-4-(trifluoromethoxy) phenylhydrazone (FCCP) was used to induce fragmentation of the mitochondrial network. In FCCP-treated neurons, mitochondria showed a distinct spherical shape which were significantly shorter in length when compared with control (Fig. 1b-d). Notably, there was also a

reduction in both volume and number of mitochondria in FCCP-induced fragmented mitochondria (Fig. 1e & h; $p < 0.001$), which was not found to be the case in Aβ − treated neurons. In addition, FCCP-treated fragmented mitochondria displayed significantly lower aspect ratio and higher circularity than mitochondria in neurons treated with control and Aβ (Fig. 1f-g).

It is important to note that although there were significant changes in mitochondrial length, aspect ratio, and circularity in neurons after exposure to Aβ or FCCP, Aβ-induced granular mitochondria was significantly different from spherical mitochondria resulting from FCCP treatment in all shape parameters measured (Fig. 1). While FCCP-induced mitochondrial fragmentation showed a distinct spherical shape accompanied by a reduction in size, Aβ appeared to induce granular mitochondria without affecting mitochondria size (Fig. 1). Hence, it is evident that Aβ-treated granular mitochondria are morphologically distinct from classic mitochondrial fragmentation. Taken together, mitochondria changed from a long and interconnected tubular network to "granular-shaped" which are morphologically distinct from the classic spherical mitochondria in mitochondrial fragmentation (Fig. 1 & S1).

To further characterize if Aβ-induced changes in mitochondrial morphology is a transient process towards fragmentation, neurons were treated with Aβ for a longer period i.e. 48 h to reveal long-term effects of Aβ on mitochondrial morphology (Figs. S2–3). Consistent with the presence of granular mitochondria at 4 h, changes in mitochondrial morphology in terms of length, aspect ratio and circularity with no significant changes in the total volume, number of mitochondria (Fig. S3) and mitochondrial content (Fig. S2) were observed when compared with the control. More importantly, mitochondria following 48 h of Aβ exposure were also found to be significantly different from FCCP-induced fragmented spherical mitochondria (Fig. S3b-g). These results confirmed that Aβ-induced granular mitochondria at early time points was not a momentary state to fragmentation and indeed persists for a long period of time in the presence of Aβ.

3.2. Granular mitochondria are functionally distinct from mitochondrial fragmentation

Mitochondrial fragmentation has often been linked with apoptosis [26]. Since granular and fragmented mitochondria shared certain degrees of morphological similarities i.e. reduction in aspect ratio and increased circularity, albeit to a different extent, we questioned whether granular mitochondria were also functionally impaired. In response to apoptotic stimuli, a reduction of mitochondrial membrane potential ($\Delta\Psi_m$) causes rupture of the outer mitochondrial membrane, which subsequently initiates the mitochondria-mediated intrinsic pathway of apoptosis [45]. Mitochondrial membrane potential was monitored by the fluorescence intensity of tetramethylrhodamine, ethyl ester (TMRE). While $\Delta\Psi_m$ was significantly reduced in FCCP-treated mitochondria, $\Delta\Psi_m$ remained intact within 6 h of Aβ treatment (Fig. 2a-b). Apart from changes in membrane potential if apoptosis really occurs, induction of apoptosis promotes the translocation of the pro-apoptotic Bcl-family protein Bax (B-cell lymphoma 2 (Bcl-2)-associated X protein) from the cytoplasm to mitochondria to form foci with Drp1 and Mfn2 to facilitate fission [46]. In order to investigate if Bax is associated with granular mitochondria, hippocampal neurons were co-transfected with EGFP-Bax and mito-RFP. It was found that following 1–6 h of Aβ treatment, Bax remained in the cytoplasm (Fig. 2d-e). In addition, there was no significant change in the expression levels of the apoptotic marker, cleaved caspase-3, following exposure to Aβ (Fig. 2f-g). These data demonstrated that Aβ-induced granular mitochondria were not associated with the initiation of apoptosis.

Although granular mitochondria were shown to be distinct from fragmented mitochondria found in apoptosis, we also examined other aspects of organelle functions in Aβ-induced granular mitochondria compared with FCCP-treated fragmented mitochondria. Production of ATP is an important indicator of mitochondrial function. While ATP production was disturbed in FCCP-treated fragmented mitochondria, as revealed by a significant increase in the ADP/ATP ratio, the ADP/ATP ratio remained stable after 1–6 h of Aβ treatment (Fig. 2c). This suggests that granular mitochondria maintained their ability to supply energy for neurons despite changes in morphology. The endoplasmic reticulum (ER)-mitochondria interaction is essential for proper function and morphology of the two organelles [47–49]. In addition, our laboratory has previously reported collapse of the ER network following Aβ treatment [40]. Owing to the intimate relationship between the two organelles, we investigated whether early change of mitochondrial morphology could cause dissociation of mitochondria from the ER, thereby affecting mitochondrial function. Primary hippocampal neurons were co-transfected with mito-GFP and ER-targeted RFP (ER-RFP). No significant change in the co-localization level between ER and mitochondria was detected after Aβ treatment, indicating that the interaction between the two organelles remained intact despite drastic changes in mitochondrial morphology (Fig. S4). In contrast, induction of mitochondrial fragmentation with FCCP substantially reduced the co-localization between the ER and mitochondria (Fig. S4). In sum, as opposed to fragmented mitochondria, granular mitochondria maintained functional integrity as well as ER-mitochondria tethering, and are not associated with apoptosis.

3.3. Aβ impairs mitochondrial dynamics without changes in fission/fusion protein expression

With no significant change in mitochondrial function in the presence of morphological changes, we went on to study whether changes in mitochondrial morphology was due to disruptions in fission and fusion, the two opposing processes that tightly regulate mitochondrial morphology [8]. Fission and fusion imbalance has also been implicated in a number of neurodegenerative diseases including AD [50].

In our study, expression levels of various fission/fusion-mediating proteins such as Drp1, OPA1, Mfn1, and Mfn2 all remained stable after 1–6 h of Aβ treatment (Fig. S5). Phosphorylation of Drp1 at Ser616 has been reported to activate Drp1-mediated fission and translocation of Drp1 has also been suggested to be a critical step to initiate fission [51]. However, no significant change in the level of phospho-Drp1^{Ser616} (Fig. S5) and the mitochondrial Drp1: cytosolic Drp1 ratio (Fig. S6b & d) was detected after Aβ treatment. These data suggest that Aβ-induced formation of granular mitochondria does not involve changes in the expression of common fission and fusion proteins.

Since expression of fission and fusion proteins in neurons was not altered after exposure to Aβ, mitochondrial dynamics was quantified in hippocampal neurons co-transfected with mito-RFP and mitochondria-targeted photoactivable GFP (mito-PAGFP). The region of interest was simultaneously photobleached and photoactivated by two-photon excitation. Simultaneous photoactivation of mito-PAGFP and fluorescence recovery after photobleaching (FRAP) imaging of mito-RFP (SPA-FRAP) allows for a novel two-way measurement of mitochondria dynamics. Both the diffusion rate of mito-PAGFP and fluorescence recovery rate of mito-RFP were significantly slower than that of controls (Fig. 3a-c; $p = 0.004$ and $p = 0.0139$, respectively), suggesting that mitochondrial dynamics was impaired following Aβ treatments at early time points. Although axonal transport of mitochondria appears to slow down after Aβ treatment, mitochondria speed was not significantly different from control (Fig. 3d).

Therefore, although no changes in the expression of fission/fusion-mediating proteins were found, there was a significant impairment in mitochondria dynamics in Aβ treated neurons.

3.4. Accumulation of reactive oxygen species in mitochondria as the triggering factor of granular mitochondria

Previous studies have implicated the role of oxidative stress in

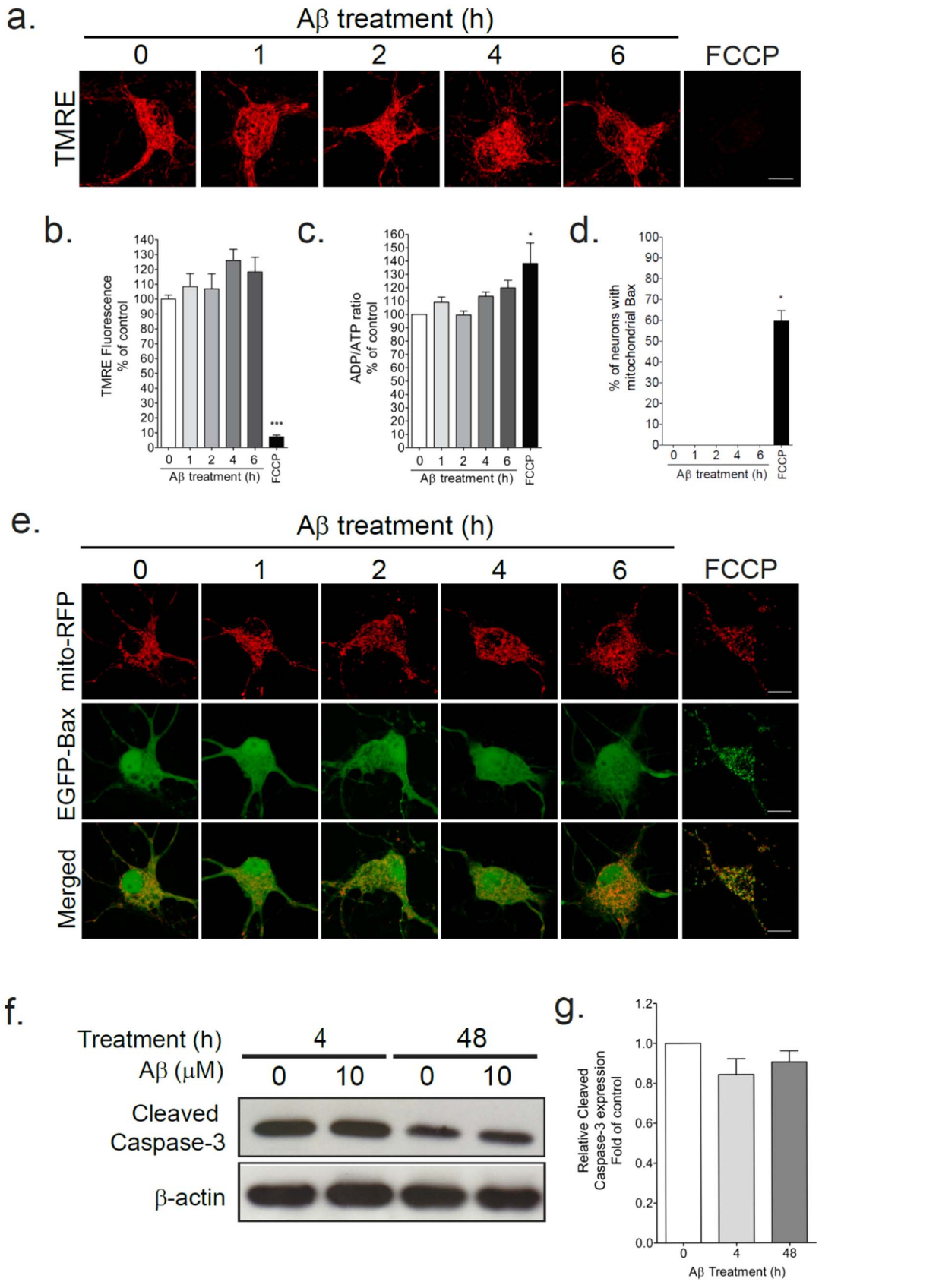

(caption on next page)

Fig. 2. Aβ-induced granular mitochondria maintain functional integrity and are not associated with apoptosis. (a) Representative confocal images of hippocampal neurons loaded with TMRE, for the determination of mitochondrial membrane potential, and treated with 10 μM Aβ for the indicated periods (in h) or 10 μM FCCP for 2 h (Scale bar: 10 μm). (b) Statistical quantification of mitochondrial membrane potential for each condition, calculated from z-axis confocal stacks. $^{***}p < 0.001$ compared with control, Kruskal-Wallis test. Data represent mean ± SEM of 4 independent experiments. (c) Statistical quantification of ADP/ATP ratio following 10 μM Aβ for the indicated periods (in h) or 10 μM FCCP for 2 h. $^{*}p < 0.05$ compared with control, Kruskal-Wallis test. Data represent mean ± SEM of 6 independent experiments. (d) Quantification of the percentage of neurons with mitochondrial Bax in primary hippocampal neurons co-transfected with EGFP-Bax and mito-RFP and treated with 10 μM Aβ for the indicated time (h). (e) Representative confocal images of primary hippocampal neurons co-transfected with mito-RFP and EGFP-Bax and treated with 10 μM Aβ for the indicated periods (in h) or 10 μM FCCP for 2 h (Scale bar: 10 μm). (f-g) Western blot analysis of cleaved caspase-3 in primary hippocampal neurons treated with 10 μM Aβ for 4 and 48 h. Quantification of western blot analysis showed no significant difference in the expression level of cleaved caspase-3 in neurons treated with 10 μM Aβ for 4 and 48 h ($p = 0.1073$), Kruskal-Wallis test. Data represent mean ± SEM of at least 3 independent experiments.

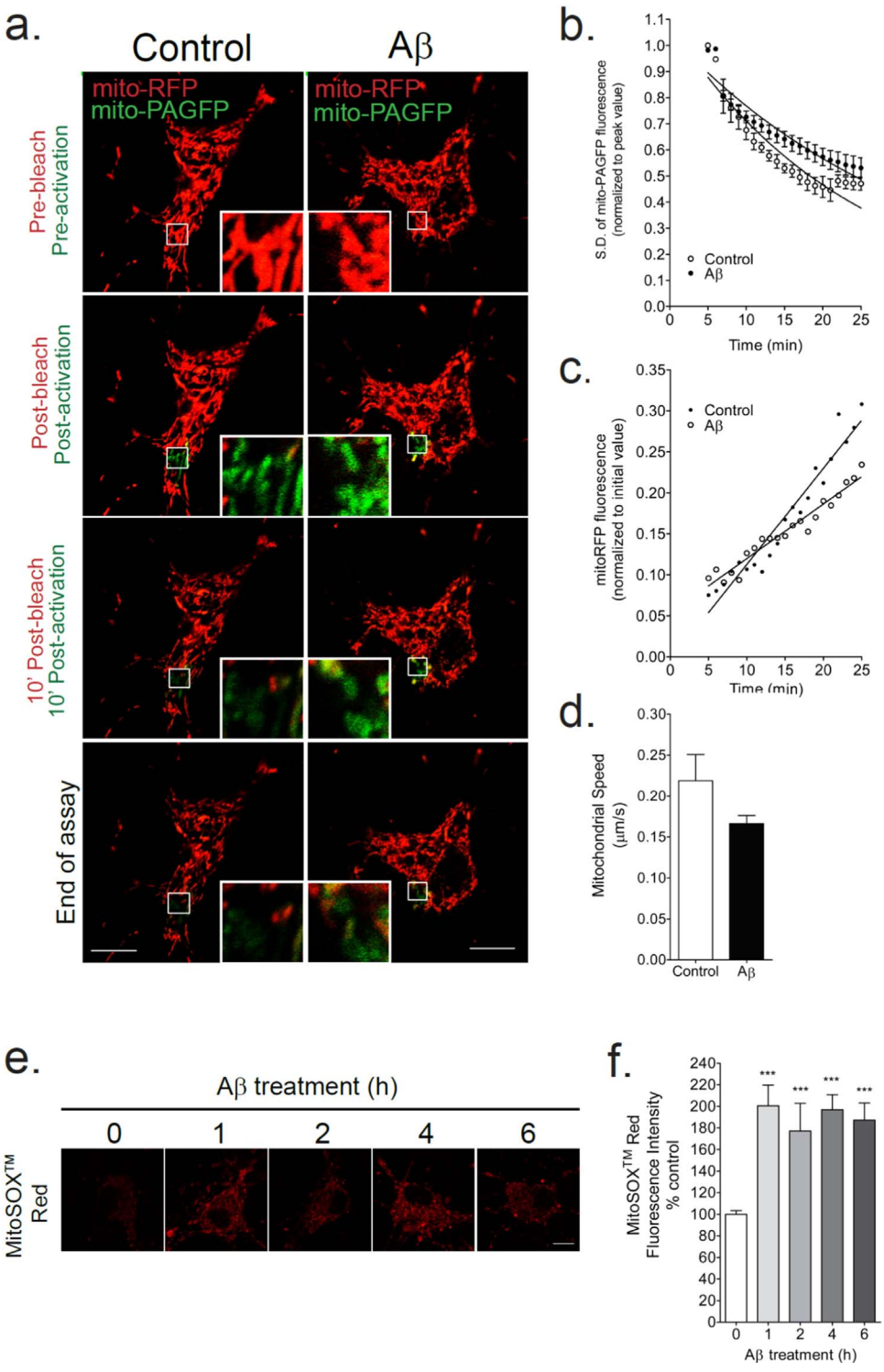

Fig. 3. Aβ induced increase in mitochondrial superoxide, and impairment in mitochondria dynamics. (a-b) Representative confocal images of hippocampal neurons loaded with MitoSOX™ Red to detect superoxide concentration in mitochondria, and treated with 10 μM Aβ for the indicated periods (in h) (Scale bar: 10 μm). Statistical quantifications of MitoSOX™ Red fluorescence intensity for each condition, calculated from z-axis confocal stacks, respectively. $^{***}p < 0.001$ compared with control; Kruskal-Wallis test and one way ANOVA test where applicable. Data represent mean ± SEM of 3 independent experiments. (c-e) Quantification of mitochondrial dynamics by simultaneous photoactivation and fluorescence recovery after photobleaching (SPA-FRAP). Representative confocal images of primary hippocampal neurons co-transfected with mito-RFP and mito-PAGFP and treated with 10 μM Aβ for 4 h (Scale bar: 10 μm). The region of interest (as shown by the boxed area) was irradiated with an 800 nm laser using two-photon excitation to achieve photobleaching of mito-RFP and photoactivation of mito-PAGFP simultaneously. The irradiation site is shown in the magnified image. (d-e) Quantification of mitochondrial dynamics using SPA-FRAP by measuring the diffusion rate of mito-PAGFP fluorescence and recovery rate of mito-RFP fluorescence ($p = 0.004$ and $p = 0.0139$ respectively). Data represent mean ± SEM of at least 4 independent experiments. (f) Quantification of mitochondria axonal transport following Aβ treatment. No significant change in the speed of mitochondria was detected following 4 h Aβ treatment. $p = 0.1658$ compared with control, Mann Whitney test. Data represent mean ± SEM of 5 independent experiments.

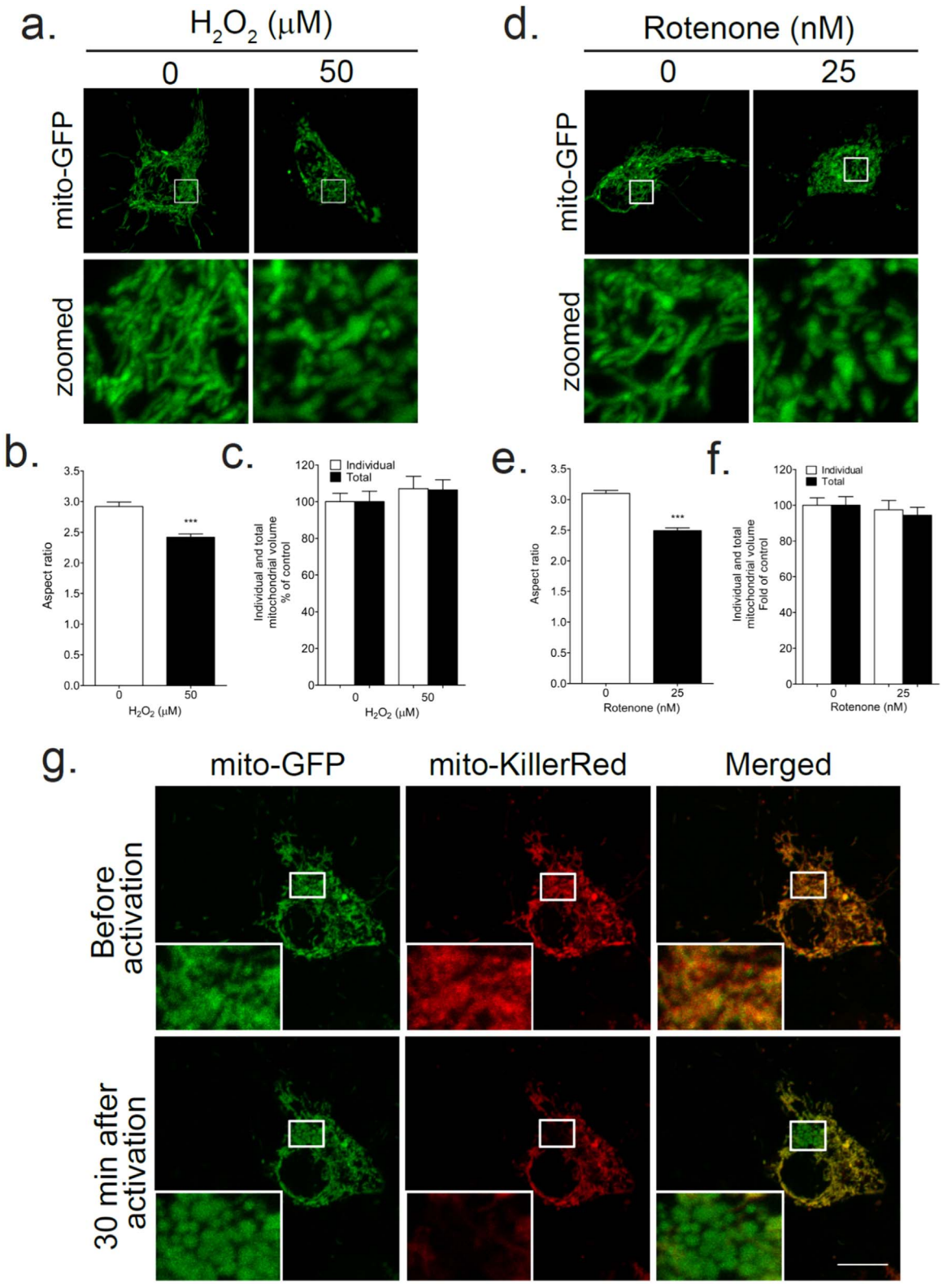

Fig. 4. Oxidative stress induces changes in mitochondria morphology comparable to Aβ treatment. (a & d) Representative confocal images of hippocampal neurons expressing mito-GFP treated with H_2O_2 and rotenone at the specified concentrations for 1 h, respectively (Scale bar: 10 μm). Images in the bottom row represent magnification of the boxed areas in the upper row (Scale bar: 2 μm). (b-c & e-f) Quantification of mitochondria volume and aspect ratio in neurons treated with H_2O_2 and rotenone, respectively. $^{***}p < 0.001$ compared with control, Kruskal-Wallis test, Dunn's multiple comparison *post-hoc* test. Data represent mean ± SEM of at least 3 independent experiments. (g) Representative confocal images of primary hippocampal neurons co-transfected with mito-GFP and mitochondria-targeted photosensitizer mito-KillerRed. The irradiated area is indicated with a square, which is shown in the magnified image. Representative images from 3 independent experiments are shown.

mitochondrial dynamics [22,24,29]. Accumulation of ROS has also been suggested as one of the earliest events in AD pathogenesis [52,53]. Increase in mitochondrial oxidative stress in neurons following exposure to Aβ was supported by a significant elevation in fluorescence intensity of the mitochondria-specific superoxide indicator MitoSOX™ Red upon 1 h Aβ treatment (Fig. 3e-f). Hence, oxidative stress may be one of the initiating events in triggering the formation of granular mitochondria after exposure to Aβ.

Although exposure to Aβ did not induce a change in fission and fusion proteins expression, Aβ did induce an increase in oxidative stress within mitochondria, leading us to examine whether the change in mitochondrial dynamics was initiated by the presence and accumulation of mitochondrial ROS. The putative oxidative stress-inducing agents H_2O_2 and rotenone was applied to primary hippocampal neurons to investigate the effects of mild oxidative stress on mitochondrial dynamics. In hippocampal neurons expressing mito-GFP, we found that 50 μM H_2O_2 and 25 nM rotenone were able to induce reductions in aspect ratios without a change in volume (Fig. 4a-f), resulting in granular mitochondria as observed in Aβ-treated cells. To further confirm the role of oxidative stress on mitochondrial morphology, we induced mitochondria-specific ROS production using the mitochondria-targeted photosensitizer KillerRed-dMito (mito-KillerRed). Mito-KillerRed has been shown to induce mitochondria-specific oxidative stress upon green light irradiation at 540–580 nm [54,55]. A localized change in mitochondrial morphology from tubular to granular shape was found in the region of interest shortly after laser irradiation (Fig. 4g). The results further confirm that oxidative stress contributes to the changes in mitochondrial morphology induced by Aβ.

3.5. Reciprocal relationship between mitochondria morphology and superoxide accumulation

To further confirm if mitochondrial oxidative stress is critical in the induction of granular mitochondria, neurons were pre-incubated with the mitochondria-targeted superoxide scavenger, mitoTEMPO, for 1 h prior to Aβ treatment. MitoTEMPO significantly attenuated Aβ-induced increases in mitochondrial superoxide concentration to a level similar to control (Fig. 5a-b). Also, mitoTEMPO significantly attenuated the reduction in mitochondrial aspect ratio induced by Aβ (Fig. 5c-d). These results indicate that mitochondrial superoxide is involved in the induction of granular mitochondria by Aβ.

Overexpression of the dominant negative mutant $Drp1^{K38A}$ has been shown to inhibit the GTPase activity of Drp1, hence inhibiting fission. Interestingly, overexpression of $Drp1^{K38A}$ also inhibited the morphological change induced by Aβ, and no significant change in mitochondria aspect ratio was detected in Aβ-treated neurons when compared with control (Fig. 5e-f). These results indicate that Aβ-induced granular mitochondria are likely to be Drp1-dependent. Treatment with mitochondrial division inhibitor 1 (mdivi-1) to inhibit Drp1 polymerization and thus attenuate Drp1-dependent mitochondrial fission [56] was used to further confirm the role of Drp1 in granular mitochondria formation. Pre-treatment of mdivi-1 abolished the induction of granular mitochondria by Aβ (Fig. 5c-d). Intriguingly, pre-treatment with mdivi-1 and overexpression of $Drp1^{K38A}$ also abolished the increase in mitochondrial superoxide concentration induced by Aβ (Fig. 5a-b & g-h). Similarly, pre-treatment with mitochondrial fusion promoter M1 (MFPM1) [57] also attenuated granular mitochondria formation and superoxide accumulation in neurons exposed to Aβ (Fig. S7). Therefore, ROS accumulation results in changes in mitochondrial morphology and most importantly, modulation of mitochondrial morphology at early time points can reduce oxidative stress. Most importantly, we have shown that there is a reciprocal relationship between mitochondria morphology and oxidative stress in Aβ treated neurons.

4. Discussion

In the present study, we have shown that Aβ induced early morphological change of mitochondria into granular shape which are morphologically and functionally distinct from spherical mitochondria seen in classic apoptosis-related mitochondrial fragmentation. Most importantly, we have shown a reciprocal relationship between ROS and mitochondrial dynamics at early stages of neurodegeneration. Mitochondrial ROS is found to disturb mitochondrial dynamics and play an important role in the induction of granular mitochondria by Aβ. MitoTEMPO attenuates the induction of mitochondria following Aβ treatment. Conversely, genetic and pharmacological manipulation of fission also diminishes the level of ROS in mitochondria. The induction of granular mitochondria by Aβ at early time points is likely to be reversible and normal tubular mitochondria morphology can be restored by manipulations of mitochondrial ROS as well as mitochondrial dynamics.

Mitochondria are particularly important in neurons owing to the high-energy demand for neuronal synaptic transmission [58]. Mitochondrial dysfunction, often described as impairment of the electron transport chain, increased production of ROS and altered mitochondrial dynamics, is a prominent feature in neurodegeneration [2,3]. In particular, recent studies have highlighted the crucial role of mitochondrial dynamics in health and diseases [59–61]. In normal conditions, the dynamic feature of mitochondria enables them to travel along the axons and deliver energy to the synapses located at the far ends of a neuron [62,63]. In response to apoptotic stimuli, as seen in neurodegeneration, mitochondria undergo fragmentation in which filamentous mitochondria break into punctate spheres [64].

Traditionally, apoptosis-associated fragmentation of the mitochondrial network has been seen as a sign of mitochondrial dysfunction at late stages of neurodegeneration. However, disturbance in mitochondrial dynamics and oxidative damage have been shown as early events in AD pathogenesis prior to substantial neuronal death [65]. In this study, we have demonstrated that a change in mitochondrial shape at early stages of neurodegeneration does not necessarily result in mitochondria dysfunction. Notably, we characterized a unique form of granular mitochondria induced by Aβ at early time points which is distinct from Aβ-triggered mitochondrial fragmentation as previously described (Fig. 1). Despite the change in morphology, $\Delta\Psi_m$ and ATP production remained stable at early time points following Aβ treatment, implying that granular mitochondria are not functionally defective (Fig. 2). Furthermore, ER-mitochondria co-localization remained unchanged (Fig. S4). Thus, Aβ-induced granular mitochondria are morphologically and functionally distinct from classic mitochondrial fragmentation in apoptosis. Previous studies have emphasized on the relationship between mitochondrial fragmentation and organelle dysfunction in neurodegeneration. However, here we show that mitochondria maintain their normal functioning at early stages of disease despite a change in morphology. Indeed, this unique granular shape was also found following prolonged Aβ treatment and is not a mere transition state toward fragmentation (Fig. S3).

The purpose of mitochondrial remodelling into granular shape remains elusive. Recent reports have shown that in stress conditions and starvation-induced macroautophagy, mitochondria elongate to promote cell survival and protect themselves from autophagosomal degradation [20,44]. Furthermore, mitochondria have been shown to display a “donut-like” toroidal shape during hypoxia-reoxygenation stress [21]. It is possible that different cellular stressors at different stages of disease progression induce different changes in mitochondria morphology as a protective mechanism. Interestingly, in primary cultured neurons under the same treatment condition, those exhibit mitochondrial Bax showed a significantly lower mitochondrial aspect ratio than those with cytosolic Bax (Fig. S9). This implies that the transition of mitochondrial morphology to granular shape might be a possible protective mechanism for neurons. Mitochondrial network remodelling to

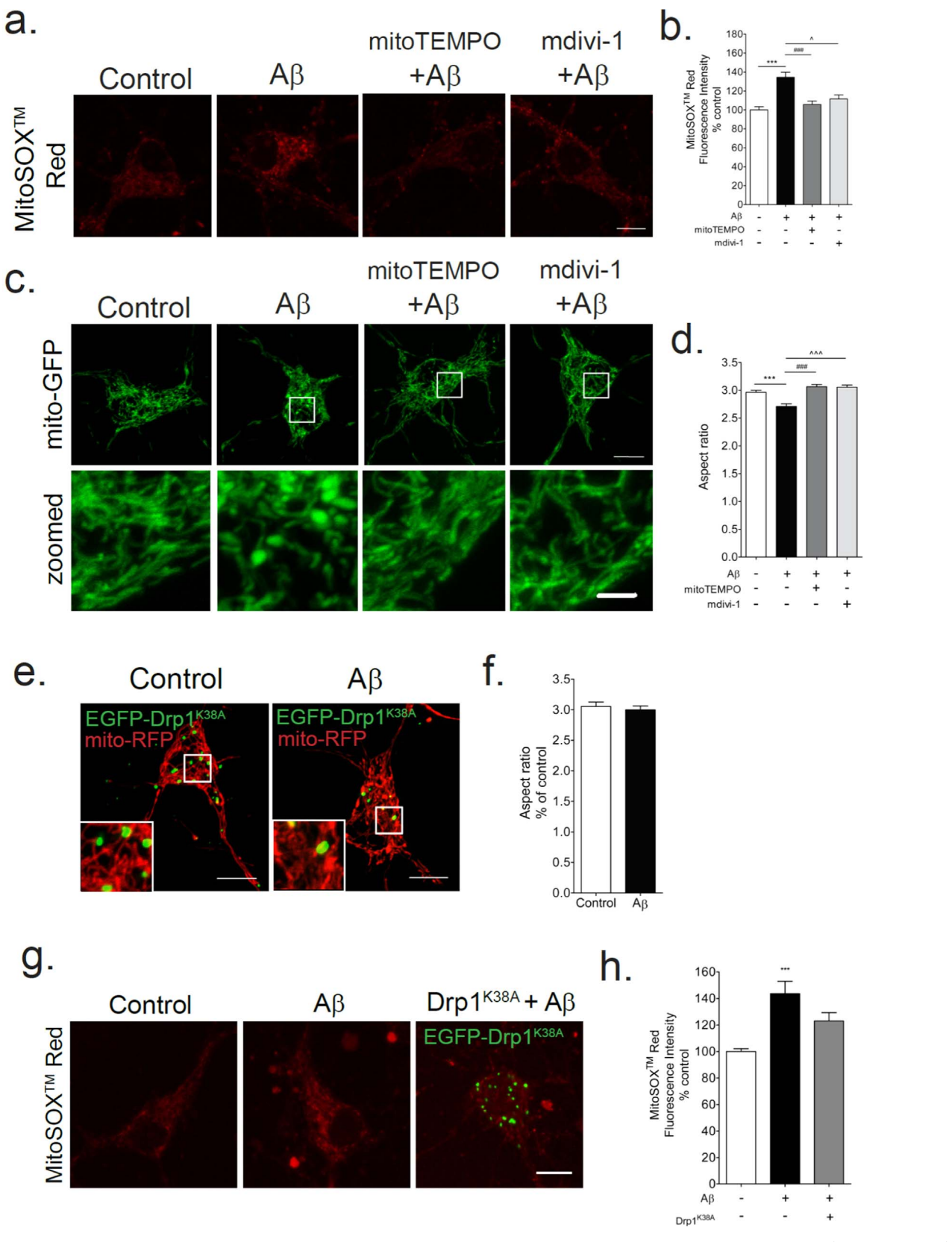

(caption on next page)

irreversible fragmentation as observed in neurodegeneration may not be a straightforward process.

The morphology of mitochondria is tightly regulated by the balance between fission and fusion. Although we found no change in the expression level of common fission and fusion proteins (Fig. 3a), Aβ was confirmed to disrupt mitochondrial dynamics by imaging experiments (Fig. 3b-d). Traditionally, mitochondrial dynamics are quantified using FRAP imaging or photoactivable GFP, independently [20,66,67]. To the

Fig. 5. Aβ-induced ROS accumulation and change in mitochondria morphology can be restored with mitochondria-targeted superoxide scavenger mitoTEMPO and pharmacological and genetic manipulations of Drp1 activity. (a) Representative confocal images of primary hippocampal neurons, expressing MitoSOX™ Red, treated with 10 μM Aβ for 4 h and pre-treated with 2.5 μM mitochondria-targeted superoxide scavenger mitoTEMPO or 5 μM mitochondrial division inhibitor 1 mdivi-1 for 1 h as indicated. (b) Quantification of MitoSOX™ Red fluorescence intensity with or without 10 μM Aβ, mdivi-1, or mitoTEMPO treatment as indicated. $^{\wedge}p < 0.05$, $^{***}/^{\#\#\#}p < 0.001$, Kruskal-Wallis test and Dunn's multiple comparison *post-hoc* test where applicable. Data represent mean ± SEM of at least 4 independent experiments (c) Representative confocal images of primary hippocampal neurons, expressing mito-GFP, treated with 10 μM Aβ for 4 h and pre-treated with mitochondria-targeted superoxide scavenger mitoTEMPO or mitochondrial division inhibitor 1 (mdivi-1) for 1 h as indicated (Scale bar: 10 μm). Images in the bottom row represent magnification of the boxed areas in the upper row (Scale bar: 2 μm). (d) Quantification of mitochondrial aspect ratio with or without 10 μM Aβ (4 h) treatment and mdivi-1 (1 h) or mitoTEMPO (1 h) pre-treatment as indicated. $^{***}/^{\#\#\#}/^{\wedge\wedge\wedge}p < 0.001$, one way ANOVA test and Tukey's multiple comparison *post-hoc* test where applicable. Data represent mean ± SEM of at least 4 independent experiments. (e) Representative confocal images of hippocampal neurons co-transfected with EGFP-Drp1^{K38A} and mito-RFP and treated with 10 μM Aβ (4 h) (Scale bar: 10 μm.). Boxed area is magnified in the image below. (f) Quantification of mitochondrial aspect ratio in primary hippocampal neurons co-transfected with EGFP-Drp1^{K38A} and mito-RFP and treated with 10 μM Aβ (4 h). Data represent mean ± SEM of at least 3 independent experiments. (g) Representative confocal images of MitoSOX™ Red loaded hippocampal neurons with and without transfection with EGFP-Drp1^{K38A} after treatment with 10 μM Aβ (4 h) (Scale bar: 10 μm.). (h) Quantification of MitoSOX™ Red intensity in 10 μM Aβ (4 h) treated primary hippocampal neurons with and without EGFP-Drp1^{K38A} expression. $^{***}p < 0.001$, Kruskal-Wallis test and Dunn's multiple comparison *post-hoc* test where applicable. Data represent mean ± SEM of at least 3 independent experiments.

best of our knowledge, this is the first study to combine both photoactivation and FRAP together using SPA-FRAP as a two-way and comprehensive measurement of mitochondrial dynamics. As shown by SPA-FRAP imaging experiments, Aβ reduced the rate of mitochondrial dynamics, which contributes to the formation of granular mitochondria (Fig. 3b-d).

In addition to a change of mitochondrial dynamics, an accumulation of ROS was found in granular mitochondria (Fig. 4a). In the present study, oxidative stress in mitochondria was found to be the triggering factor for the change in mitochondrial shape. Previous studies have shown that H_2O_2 and various oxidative stress-inducing agents can induce the classic fragmented morphological changes of mitochondria [22–24,29]. In our study, we provided evidence that direct application of oxidative stress inducing agents such as H_2O_2 and rotenone induced granular mitochondria, similar to those observed following exposure to Aβ (Fig. 5a-f). We have also demonstrated that induction of mitochondria-specific oxidative stress by laser irradiation resulted in an immediate and localized change in mitochondrial morphology (Fig. 5g). Our findings support the induction of granular mitochondria as a response against increased mitochondrial oxidative stress induced by Aβ. Notably, our study has highlighted the role of superoxide in mitochondrial dynamics and AD pathogenesis. Superoxide is a by-product from ATP production and is a major cause of oxidative stress. Overexpression of the mitochondrial antioxidant enzyme superoxide dismutase (SOD-2) has been shown to reduce hippocampal superoxide concentration and ameliorate memory deficits in an AD mouse model [68]. Furthermore, reduction in mitochondrial SOD-2 activity has been shown to promote AD-like pathology in APP transgenic mice [69]. In our study, Aβ-induced granular mitochondria can be attenuated by mitoTEMPO, which demonstrates the crucial role mitochondrial superoxide in maintaining mitochondrial morphology. Therapies targeting mitochondrial superoxide can be a potential pharmacological target for neurodegenerative diseases including AD.

Interestingly, the induction of granular mitochondria by Aβ can also be attenuated by both genetic and pharmacological manipulations of Drp1 activity. Inhibition of the GTPase activity of Drp1 by overexpression of the dominant negative mutant Drp1^{K38A} and pre-treatment of mdivi-1 abolished the induction of granular mitochondria by Aβ (Fig. 5c-f). These results suggest that Drp1 plays a role in the induction of granular mitochondria. Intriguingly, pre-incubation of mitochondria-targeted superoxide scavenger mitoTEMPO also inhibited the change in mitochondrial morphology by Aβ (Fig. 5c-d). The role of oxidative stress in the modification of mitochondrial morphology has been implicated previously. However, not many studies have investigated the opposite effect. In line with our findings, TEMPO-L, a cell permeable superoxide scavenger, has been shown to prevent mitochondrial fragmentation in mouse coronary endothelial cells isolated from diabetic mice [70]. Results from our study show that oxidative stress and mitochondrial morphology reciprocally affect each other. Application of oxidative stress-inducing agents resulted in the formation of granular mitochondria while reduction of mitochondrial oxidative stress by mitoTEMPO resulted in the restoration of granular mitochondria back to tubular-shape (Fig. 5a-f, c-d). This confirms the crucial role of ROS on the regulation of mitochondrial morphology. In an opposite condition, we have also shown that by inhibiting Drp1-dependent fission, mitochondrial superoxide concentrations would return to a level similar with controls (Fig. 5a-b). In agree with our results, a recent study has shown that P110, a selective inhibitor which blocks Drp1 enzyme activity and Drp1/Fis1 interaction, attenuated MPP^+-induced increases in mitochondrial superoxide levels [71]. Another study by Kim et al. also showed that mdivi-1 inhibited Aβ-induced ROS [72]. Although we did not observe significant changes in the expression level of Drp1 and Drp1 translocation to mitochondria following mitoTEMPO and mdivi-1 treatments (Fig. S6a), it is evident that mitochondrial dynamics and ROS affect one another. It is not clear if Drp1 and superoxide directly interact with each other or through secondary responses to affect mitochondrial morphology in response to an accumulation of ROS in mitochondria, although previous findings have suggested a direct interaction between superoxide and mitochondrial morphology [70]. Intriguingly, pre-treatment of the fusion promoter MFPM1 was also found to attenuate the changes in mitochondrial morphology and ameliorate increased superoxide concentration as induced by Aβ, suggesting mitochondrial elongation by either inhibiting fission or promoting fusion can affect mitochondrial ROS. Our study has provided a new perspective on how manipulations of mitochondrial dynamics can affect mitochondrial ROS level, and vice versa.

Currently, it is debatable on whether oxidative stress is the cause or consequence of neurodegeneration. Our study has shown that increased oxidative stress preceded mitochondrial dysfunction as well as apoptosis in an in vitro model of AD (Figs. 2 and 3). ROS accumulation can be found prior to the formation of classic spherical mitochondria as seen in apoptosis, and the increase in ROS can be diminished by mitochondria-targeted antioxidant mitoTEMPO and manipulation of mitochondria fission or fusion by mdivi-1 and MFPM1 (Fig. 5 & S7). Mitochondrial ROS and dynamics have been demonstrated and proposed as new targets for therapeutic intervention for neurodegeneration [65,73–75]. Given the mutual relationship between ROS and mitochondrial dynamics, this may provide a novel effective pharmacological target for neurodegenerative and other human diseases.

5. Conclusions

Our study showed that at early stages of neurodegeneration, beta-amyloid (Aβ) induced morphological changes in mitochondria where they become granular shape which was distinct from the conventional round and fragmented mitochondria in terms of both morphology and function. In addition, we demonstrated that accumulation of mitochondrial reactive oxygen species triggered granular mitochondria formation, while mitoTEMPO (a mitochondria-targeted superoxide scavenger) restored tubular mitochondrial morphology within Aβ-treated neurons. Interestingly, modulations of mitochondria fission and fusion by genetic and pharmacological means not only attenuated the induction of granular mitochondria, but also diminished mitochondrial superoxide levels in Aβ-treated neurons. This study demonstrates a

unique reciprocal relationship between mitochondrial dynamics and reactive oxygen species and provides a new possible therapeutic target at early stages of neurodegenerative disease pathogenesis.

Author's contributions

CHLH and RCCC conceived the study and designed the experiments. CHLH performed the experiments and data analysis. CHLH and YTC. performed the mitochondrial morphometric analysis. CHLH and SSYC participated in data interpretation. CHLH, SSYC and RCCC wrote the manuscript with help from all authors. YSH, SMYL and RCCC obtained funding to support the study.

Acknowledgement

We thank Prof. S.K. Kong, Dr. Z. Dong and Dr. R. Youle for kindly providing the constructs used in the study. The study was partially supported by HKU Seed Funding for Basic Research (201511159237 & 201611159183), Health and Medical Research Fund (02131956) from Food and Health Bureau of Hong Kong SAR Government, HKU Alzheimer's Disease Research Network under Strategic Research Theme on Ageing, generous support from Ms. Kit-Wan Chow to RCCC. All the imaging experiments were supported by the Faculty Core Facility at the LKS Faculty of Medicine, HKU. Research support to SMYL is grants from the Science and Technology Development Fund of Macao SAR (Ref. No FDCT134/2014/A3) and Research Committee-University of Macau (MYRG2016-00129-ICMS-QRCM). Research support to YSH is grants from Hong Kong Polytechnic University G-YBRO and 1-ZE5L.

Appendix A. Supplementary material

Supplementary data associated with this article can be found in the online version at http://dx.doi.org/10.1016/j.redox.2017.08.010.

References

[1] S.J. Baloyannis, Mitochondrial alterations in Alzheimer's disease, J. Alzheimers Dis. 9 (2006) 119–126.
[2] M.F. Beal, Mitochondria take center stage in aging and neurodegeneration, Ann. Neurol. 58 (2005) 495–505.
[3] M.T. Lin, M.F. Beal, Mitochondrial dysfunction and oxidative stress in neurodegenerative diseases, Nature 443 (2006) 787–795.
[4] F.A. Cabezas-Opazo, K. Vergara-Pulgar, M.J. Perez, C. Jara, C. Osorio-Fuentealba, R.A. Quintanilla, Mitochondrial dysfunction contributes to the pathogenesis of Alzheimer's disease, Oxid. Med. Cell. Longev. 2015 (2015) 509654.
[5] X. Zhu, G. Perry, M.A. Smith, X. Wang, Abnormal mitochondrial dynamics in the pathogenesis of Alzheimer's disease, J. Alzheimers Dis. 33 (Suppl. 1) (2013) S253–S262.
[6] M.H. Yan, X. Wang, X. Zhu, Mitochondrial defects and oxidative stress in Alzheimer disease and Parkinson disease, Free Radic. Biol. Med 62 (2013) 90–101.
[7] M. Amiri, P.J. Hollenbeck, Mitochondrial biogenesis in the axons of vertebrate peripheral neurons, Dev. Neurobiol. 68 (2008) 1348–1361.
[8] J. Bereiter-Hahn, M. Voth, Dynamics of mitochondria in living cells: shape changes, dislocations, fusion, and fission of mitochondria, Microsc. Res Tech. 27 (1994) 198–219.
[9] G. Twig, A. Elorza, A.J. Molina, H. Mohamed, J.D. Wikstrom, G. Walzer, L. Stiles, S.E. Haigh, S. Katz, G. Las, et al., Fission and selective fusion govern mitochondrial segregation and elimination by autophagy, EMBO J. 27 (2008) 433–446.
[10] H. Chen, S.A. Detmer, A.J. Ewald, E.E. Griffin, S.E. Fraser, D.C. Chan, Mitofusins Mfn1 and Mfn2 coordinately regulate mitochondrial fusion and are essential for embryonic development, J. Cell Biol. 160 (2003) 189–200.
[11] S. Cipolat, O. Martins de Brito, B. Dal Zilio, L. Scorrano, OPA1 requires mitofusin 1 to promote mitochondrial fusion, Proc. Natl. Acad. Sci. USA 101 (2004) 15927–15932.
[12] F. Legros, A. Lombes, P. Frachon, M. Rojo, Mitochondrial fusion in human cells is efficient, requires the inner membrane potential, and is mediated by mitofusins, Mol. Biol. Cell 13 (2002) 4343–4354.
[13] M. Rojo, F. Legros, D. Chateau, A. Lombes, Membrane topology and mitochondrial targeting of mitofusins, ubiquitous mammalian homologs of the transmembrane GTPase Fzo, J. Cell Sci. 115 (2002) 1663–1674.
[14] A. Santel, M.T. Fuller, Control of mitochondrial morphology by a human mitofusin, J. Cell Sci. 114 (2001) 867–874.
[15] S. Gandre-Babbe, A.M. van der Bliek, The novel tail-anchored membrane protein Mff controls mitochondrial and peroxisomal fission in mammalian cells, Mol. Biol. Cell 19 (2008) 2402–2412.
[16] D.I. James, P.A. Parone, Y. Mattenberger, J.C. Martinou, hFis1, a novel component of the mammalian mitochondrial fission machinery, J. Biol. Chem. 278 (2003) 36373–36379.
[17] H. Otera, C. Wang, M.M. Cleland, K. Setoguchi, S. Yokota, R.J. Youle, K. Mihara, Mff is an essential factor for mitochondrial recruitment of Drp1 during mitochondrial fission in mammalian cells, J. Cell Biol. 191 (2010) 1141–1158.
[18] E. Smirnova, L. Griparic, D.L. Shurland, A.M. van der Bliek, Dynamin-related protein Drp1 is required for mitochondrial division in mammalian cells, Mol. Biol. Cell 12 (2001) 2245–2256.
[19] Y. Yoon, E.W. Krueger, B.J. Oswald, M.A. McNiven, The mitochondrial protein hFis1 regulates mitochondrial fission in mammalian cells through an interaction with the dynamin-like protein DLP1, Mol. Cell Biol. 23 (2003) 5409–5420.
[20] L.C. Gomes, G. Di Benedetto, L. Scorrano, During autophagy mitochondria elongate, are spared from degradation and sustain cell viability, Nat. Cell Biol. 13 (2011) 589–598.
[21] X. Liu, G. Hajnoczky, Altered fusion dynamics underlie unique morphological changes in mitochondria during hypoxia-reoxygenation stress, Cell Death Differ. 18 (2011) 1561–1572.
[22] X. Fan, R. Hussien, G.A. Brooks, H2O2-induced mitochondrial fragmentation in C2C12 myocytes, Free Radic. Biol. Med. 49 (2010) 1646–1654.
[23] M. Jendrach, S. Mai, S. Pohl, M. Voth, J. Bereiter-Hahn, Short- and long-term alterations of mitochondrial morphology, dynamics and mtDNA after transient oxidative stress, Mitochondrion 8 (2008) 293–304.
[24] S. Wu, F. Zhou, Z. Zhang, D. Xing, Mitochondrial oxidative stress causes mitochondrial fragmentation via differential modulation of mitochondrial fission-fusion proteins, FEBS J. 278 (2011) 941–954.
[25] S. Frank, B. Gaume, E.S. Bergmann-Leitner, W.W. Leitner, E.G. Robert, F. Catez, C.L. Smith, R.J. Youle, The role of dynamin-related protein 1, a mediator of mitochondrial fission, in apoptosis, Dev. Cell 1 (2001) 515–525.
[26] M. Karbowski, R.J. Youle, Dynamics of mitochondrial morphology in healthy cells and during apoptosis, Cell Death Differ. 10 (2003) 870–880.
[27] M.G. Sun, J. Williams, C. Munoz-Pinedo, G.A. Perkins, J.M. Brown, M.H. Ellisman, D.R. Green, T.G. Frey, Correlated three-dimensional light and electron microscopy reveals transformation of mitochondria during apoptosis, Nat. Cell Biol. 9 (2007) 1057–1065.
[28] F. Burte, V. Carelli, P.F. Chinnery, P. Yu-Wai-Man, Disturbed mitochondrial dynamics and neurodegenerative disorders, Nat. Rev. Neurol. 11 (2015) 11–24.
[29] M.J. Barsoum, H. Yuan, A.A. Gerencser, G. Liot, Y. Kushnareva, S. Graber, I. Kovacs, W.D. Lee, J. Waggoner, J. Cui, et al., Nitric oxide-induced mitochondrial fission is regulated by dynamin-related GTPases in neurons, EMBO J. 25 (2006) 3900–3911.
[30] X. Wang, B. Su, S.L. Siedlak, P.I. Moreira, H. Fujioka, Y. Wang, G. Casadesus, X. Zhu, Amyloid-beta overproduction causes abnormal mitochondrial dynamics via differential modulation of mitochondrial fission/fusion proteins, Proc. Natl. Acad. Sci. USA 105 (2008) 19318–19323.
[31] D.H. Cho, T. Nakamura, J. Fang, P. Cieplak, A. Godzik, Z. Gu, S.A. Lipton, S-nitrosylation of Drp1 mediates beta-amyloid-related mitochondrial fission and neuronal injury, Science 324 (2009) 102–105.
[32] D.I. Kim, K.H. Lee, J.Y. Oh, J.S. Kim, H.J. Han, Relationship between beta-amyloid and mitochondrial dynamics, Cell. Mol. Neurobiol. (2016).
[33] X. Wang, B. Su, H.G. Lee, X. Li, G. Perry, M.A. Smith, X. Zhu, Impaired balance of mitochondrial fission and fusion in Alzheimer's disease, J. Neurosci. 29 (2009) 9090–9103.
[34] M.J. Calkins, P.H. Reddy, Amyloid beta impairs mitochondrial anterograde transport and degenerates synapses in Alzheimer's disease neurons, Biochim. Biophys. Acta 1812 (2011) 507–513.
[35] L.L. Xu, Y. Shen, X. Wang, L.F. Wei, P. Wang, H. Yang, C.F. Wang, Z.H. Xie, J.Z. Bi, Mitochondrial dynamics changes with age in an APPsw/PS1dE9 mouse model of Alzheimer's disease, Neuroreport 28 (2017) 222–228.
[36] M.J. Calkins, M. Manczak, P. Mao, U. Shirendeb, P.H. Reddy, Impaired mitochondrial biogenesis, defective axonal transport of mitochondria, abnormal mitochondrial dynamics and synaptic degeneration in a mouse model of Alzheimer's disease, Hum. Mol. Genet. 20 (2011) 4515–4529.
[37] E. Trushina, E. Nemutlu, S. Zhang, T. Christensen, J. Camp, J. Mesa, A. Siddiqui, Y. Tamura, H. Sesaki, T.M. Wengenack, et al., Defects in mitochondrial dynamics and metabolomic signatures of evolving energetic stress in mouse models of familial Alzheimer's disease, PloS One 7 (2012) e32737.
[38] L. Wang, L. Guo, L. Lu, H. Sun, M. Shao, S.J. Beck, L. Li, J. Ramachandran, Y. Du, H. Du, Synaptosomal Mitochondrial dysfunction in 5xFAD mouse model of Alzheimer's disease, PLoS One 11 (2016) e0150441.
[39] B. Bossy, A. Petrilli, E. Klinglmayr, J. Chen, U. Lutz-Meindl, A.B. Knott, E. Masliah, R. Schwarzenbacher, E. Bossy-Wetzel, S-Nitrosylation of DRP1 does not affect enzymatic activity and is not specific to Alzheimer's disease, J. Alzheimers Dis. 20 (Suppl. 2) (2010) S513–S526.
[40] C.S. Lai, J. Preisler, L. Baum, D.H. Lee, H.K. Ng, J. Hugon, K.F. So, R.C.C. Chang, Low molecular weight Abeta induces collapse of endoplasmic reticulum, Mol. Cell Neurosci. 41 (2009) 32–43.
[41] R.K. Dagda, S.J. Cherra 3rd, S.M. Kulich, A. Tandon, D. Park, C.T. Chu, Loss of PINK1 function promotes mitophagy through effects on oxidative stress and mitochondrial fission, J. Biol. Chem. 284 (2009) 13843–13855.
[42] M.Y. Cha, S.H. Han, S.M. Son, H.S. Hong, Y.J. Choi, J. Byun, I. Mook-Jung, Mitochondria-specific accumulation of amyloid beta induces mitochondrial dysfunction leading to apoptotic cell death, PLoS One 7 (2012) e34929.
[43] G.L. Rintoul, A.J. Filiano, J.B. Brocard, G.J. Kress, I.J. Reynolds, Glutamate decreases mitochondrial size and movement in primary forebrain neurons, J.

Neurosci. 23 (2003) 7881–7888.
[44] A.S. Rambold, B. Kostelecky, N. Elia, J. Lippincott-Schwartz, Tubular network formation protects mitochondria from autophagosomal degradation during nutrient starvation, Proc. Natl. Acad. Sci. USA 108 (2011) 10190–10195.
[45] D.R. Green, G. Kroemer, The pathophysiology of mitochondrial cell death, Science 305 (2004) 626–629.
[46] M. Karbowski, Y.J. Lee, B. Gaume, S.Y. Jeong, S. Frank, A. Nechushtan, A. Santel, M. Fuller, C.L. Smith, R.J. Youle, Spatial and temporal association of Bax with mitochondrial fission sites, Drp1, and Mfn2 during apoptosis, J. Cell Biol. 159 (2002) 931–938.
[47] O.M. de Brito, L. Scorrano, Mitofusin 2 tethers endoplasmic reticulum to mitochondria, Nature 456 (2008) 605–610.
[48] J.R. Friedman, L.L. Lackner, M. West, J.R. DiBenedetto, J. Nunnari, G.K. Voeltz, ER tubules mark sites of mitochondrial division, Science 334 (2011) 358–362.
[49] G. Szabadkai, A.M. Simoni, M. Chami, M.R. Wieckowski, R.J. Youle, R. Rizzuto, Drp-1-dependent division of the mitochondrial network blocks intraorganellar Ca^{2+} waves and protects against Ca^{2+}-mediated apoptosis, Mol. Cell 16 (2004) 59–68.
[50] B. Su, X. Wang, L. Zheng, G. Perry, M.A. Smith, X. Zhu, Abnormal mitochondrial dynamics and neurodegenerative diseases, Biochim Biophys. Acta 1802 (2010) 135–142.
[51] N. Taguchi, N. Ishihara, A. Jofuku, T. Oka, K. Mihara, Mitotic phosphorylation of dynamin-related GTPase Drp1 participates in mitochondrial fission, J. Biol. Chem. 282 (2007) 11521–11529.
[52] W.R. Markesbery, Oxidative stress hypothesis in Alzheimer's disease, Free Radic. Biol. Med. 23 (1997) 134–147.
[53] A. Nunomura, G. Perry, G. Aliev, K. Hirai, A. Takeda, E.K. Balraj, P.K. Jones, H. Ghanbari, T. Wataya, S. Shimohama, et al., Oxidative damage is the earliest event in Alzheimer disease, J. Neuropathol. Exp. Neurol. 60 (2001) 759–767.
[54] M.E. Bulina, D.M. Chudakov, O.V. Britanova, Y.G. Yanushevich, D.B. Staroverov, T.V. Chepurnykh, E.M. Merzlyak, M.A. Shkrob, S. Lukyanov, K.A. Lukyanov, A genetically encoded photosensitizer, Nat. Biotechnol. 24 (2006) 95–99.
[55] V. Choubey, D. Safiulina, A. Vaarmann, M. Cagalinec, P. Wareski, M. Kuum, A. Zharkovsky, A. Kaasik, Mutant A53T alpha-synuclein induces neuronal death by increasing mitochondrial autophagy, J. Biol. Chem. 286 (2011) 10814–10824.
[56] A. Cassidy-Stone, J.E. Chipuk, E. Ingerman, C. Song, C. Yoo, T. Kuwana, M.J. Kurth, J.T. Shaw, J.E. Hinshaw, D.R. Green, J. Nunnari, Chemical inhibition of the mitochondrial division dynamin reveals its role in Bax/Bak-dependent mitochondrial outer membrane permeabilization, Dev. Cell 14 (2008) 193–204.
[57] D. Wang, J. Wang, G.M. Bonamy, S. Meeusen, R.G. Brusch, C. Turk, P. Yang, P.G. Schultz, A small molecule promotes mitochondrial fusion in mammalian cells, Angew. Chem. Int Ed. Engl. 51 (2012) 9302–9305.
[58] P. Verstreken, C.V. Ly, K.J. Venken, T.W. Koh, Y. Zhou, H.J. Bellen, Synaptic mitochondria are critical for mobilization of reserve pool vesicles at Drosophila neuromuscular junctions, Neuron 47 (2005) 365–378.
[59] L. Scorrano, Keeping mitochondria in shape: a matter of life and death, Eur. J. Clin. Investig. 43 (2013) 886–893.
[60] A.B. Knott, G. Perkins, R. Schwarzenbacher, E. Bossy-Wetzel, Mitochondrial fragmentation in neurodegeneration, Nat. Rev. Neurosci. 9 (2008) 505–518.
[61] D.C. Chan, Mitochondria: dynamic organelles in disease, aging, and development, Cell 125 (2006) 1241–1252.
[62] D.T. Chang, A.S. Honick, I.J. Reynolds, Mitochondrial trafficking to synapses in cultured primary cortical neurons, J. Neurosci. 26 (2006) 7035–7045.
[63] P.J. Hollenbeck, W.M. Saxton, The axonal transport of mitochondria, J. Cell Sci. 118 (2005) 5411–5419.
[64] I. Martinou, S. Desagher, R. Eskes, B. Antonsson, E. Andre, S. Fakan, J.C. Martinou, The release of cytochrome c from mitochondria during apoptosis of NGF-deprived sympathetic neurons is a reversible event, J. Cell Biol. 144 (1999) 883–889.
[65] P.H. Reddy, R. Tripathi, Q. Troung, K. Tirumala, T.P. Reddy, V. Anekonda, U.P. Shirendeb, M.J. Calkins, A.P. Reddy, P. Mao, M. Manczak, Abnormal mitochondrial dynamics and synaptic degeneration as early events in Alzheimer's disease: implications to mitochondria-targeted antioxidant therapeutics, Biochim. Biophys. Acta 1822 (2012) 639–649.
[66] T.J. Collins, M.J. Berridge, P. Lipp, M.D. Bootman, Mitochondria are morphologically and functionally heterogeneous within cells, EMBO J. 21 (2002) 1616–1627.
[67] M. Karbowski, D. Arnoult, H. Chen, D.C. Chan, C.L. Smith, R.J. Youle, Quantitation of mitochondrial dynamics by photolabeling of individual organelles shows that mitochondrial fusion is blocked during the Bax activation phase of apoptosis, J. Cell Biol. 164 (2004) 493–499.
[68] C.A. Massaad, T.M. Washington, R.G. Pautler, E. Klann, Overexpression of SOD-2 reduces hippocampal superoxide and prevents memory deficits in a mouse model of Alzheimer's disease, Proc. Natl. Acad. Sci. USA 106 (2009) 13576–13581.
[69] L. Esposito, J. Raber, L. Kekonius, F. Yan, G.Q. Yu, N. Bien-Ly, J. Puolivali, K. Scearce-Levie, E. Masliah, L. Mucke, Reduction in mitochondrial superoxide dismutase modulates Alzheimer's disease-like pathology and accelerates the onset of behavioral changes in human amyloid precursor protein transgenic mice, J. Neurosci. 26 (2006) 5167–5179.
[70] A. Makino, B.T. Scott, W.H. Dillmann, Mitochondrial fragmentation and superoxide anion production in coronary endothelial cells from a mouse model of type 1 diabetes, Diabetologia 53 (2010) 1783–1794.
[71] X. Qi, N. Qvit, Y.C. Su, D. Mochly-Rosen, A novel Drp1 inhibitor diminishes aberrant mitochondrial fission and neurotoxicity, J. Cell Sci. 126 (2013) 789–802.
[72] D.I. Kim, K.H. Lee, A.A. Gabr, G.E. Choi, J.S. Kim, S.H. Ko, H.J. Han, Abeta-Induced Drp1 phosphorylation through Akt activation promotes excessive mitochondrial fission leading to neuronal apoptosis, Biochim. Biophys. Acta 1863 (2016) 2820–2834.
[73] D.J. Bonda, M.A. Smith, G. Perry, H.G. Lee, X. Wang, X. Zhu, The mitochondrial dynamics of Alzheimer's disease and Parkinson's disease offer important opportunities for therapeutic intervention, Curr. Pharm. Des. 17 (2011) 3374–3380.
[74] J. Grohm, S.W. Kim, U. Mamrak, S. Tobaben, A. Cassidy-Stone, J. Nunnari, N. Plesnila, C. Culmsee, Inhibition of Drp1 provides neuroprotection in vitro and in vivo, Cell Death Differ. 19 (2012) 1446–1458.
[75] J. Yan, X.H. Liu, M.Z. Han, Y.M. Wang, X.L. Sun, N. Yu, T. Li, B. Su, Z.Y. Chen, Blockage of GSK3beta-mediated Drp1 phosphorylation provides neuroprotection in neuronal and mouse models of Alzheimer's disease, Neurobiol. Aging 36 (2015) 211–227.